RSC Advances

PAPER

View Article Online
View Journal | View Issue

Cite this: *RSC Adv.*, 2025, **15**, 22831

Uncovering the biosynthetic pathways of key flavor and color compounds in pomegranate using pathway-based metabolomics†

Jin-Pyo An, [a] Dongjoo Kim, [a] Xuebo Song, [a] John M. Chater,[b] Claire C. Heinitz[c] and Yu Wang *[a]

Pomegranate, a subtropical fruit renowned for its sensory appeal and nutritional benefits, has garnered global attention due to its distinctive flavor profile and putative health benefits. Enhancing fruit quality, particularly in terms of flavor, could significantly boost consumer preference and market demand. However, the development of flavor is a complex process that requires a deep understanding of the metabolic pathways that contribute to it. In this study, a comprehensive metabolomics approach employing gas chromatography mass spectrometry (GC/MS) and liquid chromatography mass spectrometry (LC/MS) techniques was used to identify flavor compounds and their precursors. To account for distinctive pomegranate compounds, anthocyanins and punicalagins were analyzed as well. Four key flavor-related pathways (shikimate/phenylpropanoid pathway, terpenoid backbone biosynthesis, lipoxygenase pathway, and tricarboxylic acid cycle metabolism) were explored to identify the regulatory mechanisms behind flavor compound production. Notably, Wonderful, a dominant cultivar in California, up-regulated most pathways to produce flavor-related secondary metabolites from their precursors. These findings offer a valuable foundation for breeding efforts aimed at improving sensory traits in pomegranate, ultimately enhancing consumer satisfaction.

Received 21st January 2025
Accepted 17th June 2025

DOI: 10.1039/d5ra00511f

rsc.li/rsc-advances

1. Introduction

The pomegranate (*Punica granatum* L.) is one of the oldest known edible fruit tree species.[1] However, despite its long history, pomegranate production was hindered for years by its inconvenient consumption, resulting in low retail attractiveness. However, in the past two decades, the pomegranate market has experienced significant growth, fueled by increasing consumer demand for fruits considered both healthy and delicious, often referred to as superfruits.[2] Pomegranates are cultivated over 835 950 hectares globally, yielding around 8.1 million metric tons.[3] In the United States, California is the top producer of pomegranates, contributing more than 90% of the country's supply, with 'Wonderful' representing the vast majority of plantings.[4]

Pomegranates' antioxidant activity and color are due to a variety of anthocyanins. Anthocyanins are a class of naturally occurring pigments found in many fruits responsible for their vibrant red, purple, and blue colors. The basic structure of anthocyanins consists of flavylium core, sugar moieties, and attached functional groups such as hydroxyl and methyl. The flavylium core is a key structural component of anthocyanins, characterized by a three-ring structure and a positively charged oxygen at a C ring.[5] The conjugated structure of the flavylium cation allows anthocyanins to donate electrons or hydrogen atoms to neutralize free radicals, reducing and preventing oxidative stress in biological systems. So far, various bioactivities have been reported, including antioxidant, anti-inflammatory, anti-cancer, and neuroprotective effects.[6]

In addition, the flavylium cation has an extensive conjugated π-electron system, which allows it to absorb visible light effectively. The positive charge on the oxygen and the conjugated system enable multiple resonance structures which allow for maximum absorption of visible light.[7] The attached functional groups, such as hydroxyl or methyl groups, further influence the color by acting as electron donors or acceptors, leading to significant shifts in hue. Anthocyanins also undergo structural transformations depending on the pH of their environment, which results in color changes. In acidic conditions, anthocyanins predominantly exist as the flavylium cation, which displays vibrant red colors due to strong absorption in the visible

[a]*Food Science and Human Nutrition Department, Citrus Research and Education Center, University of Florida, 700 Experiment Station Road, Lake Alfred, FL 33850, USA. E-mail: yu.wang@ufl.edu*

[b]*Horticultural Science Department, Citrus Research and Education Center, University of Florida, 700 Experiment Station Road, Lake Alfred, FL 33850, USA*

[c]*United States Department of Agriculture, Agricultural Research Service, National Clonal Germplasm Repository – Tree Fruit & Nut Crops & Grapes, University of California, One Shields Ave, Davis, Davis, CA 95616, USA*

† Electronic supplementary information (ESI) available. See DOI: https://doi.org/10.1039/d5ra00511f

spectrum.[8] Given that pomegranates show a naturally low pH, largely due to their high concentrations of citric and malic acids, the anthocyanins in pomegranate juice tend to exhibit especially vivid colors.

Fruit juice color is one of the most important quality traits. The perception of color can affect consumer preferences and purchasing decisions, making it a vital aspect for producers to consider. The characteristic blood-red color of pomegranate juice, combined with its rich nutritional profile, may contribute to its long-standing reputation as a "blood tonic".[9] This deep, vibrant color not only enhances its visual appeal but also reinforces its association with health and vitality. However, limited research has been conducted to quantify individual anthocyanins in California grown pomegranate.[10]

Besides fruit color, flavor compounds are crucial in defining the distinctive taste of fruits. Volatile compounds significantly influence fruit aroma, with their distribution and concentration shaping the overall flavor profile.[11] Understanding the formation and regulation of flavor compounds is essential for improving or preserving the taste of food as breeding efforts aimed at increasing yield might affect the taste. Thus, a pathway-focused metabolomics approach is crucial for uncovering the metabolic processes responsible for producing significant flavor elements in pomegranate. To date, no pathway-based metabolomics study has been conducted on California-grown pomegranate.

To reveal key flavor pathways, we conducted targeted metabolomics to profile essential primary and secondary metabolites, including organic acids, amino acids, sugars, hormones, and phenolic compounds. Additionally, we analyzed pomegranate-specific compounds such as anthocyanins, punicalagins, and flavor-related volatiles. As a result, a comprehensive dataset of 119 selected metabolites was established. This dataset enabled us to correlate the behavior of primary metabolites and pomegranate distinctive flavor compounds. This understanding sheds light on the biochemical processes that influence flavor in pomegranates, potentially assisting to identify key genes involved in these mechanisms.

2. Experimental

2.1. General chemicals

LC-MS grade acetonitrile, methanol, and water were sourced from Fisher Scientific (Fair Lawn, NJ, USA). Anthocyanin standards (cyanidin 3-glucoside, cyanidin 3,5-diglucoside, cyanidin rutinoside, delphinidin 3-glucoside, delphinidin 3,5-diglucoside, delphinidin 3-rutinoside, peonidin 3-glucoside, peonidin 3,5-diglucoside) were obtained from Sigma-Aldrich (St. Louis, MO, USA). Punicalagin, 9- and 13-hydroperoxyoctadecadienoic acid (9- and 13-HPODE) were obtained from Santa Cruz Biotechnology Inc (Dallas, Tx, USA). Jasmonic acid, jasmonoyl isoleucine (JA-Ile), 9,10-dihydro jasmonic acid, *cis*-(+)-12-oxophytodienoic acid (OPDA), gibberellic acid, 2-*C*-methyl-*D*-erythritol 4 phosphate, naringenin, neohesperidin, rutin, hesperidin, eriodictyol, eriocitrin, mevalonic acid, coumaric acid, cinnamic acid, phenylalanine, arginine, lysine, valine, tyrosine, proline, alanine, serine, glutamic acid, threonine, histidine, shikimic acid, pyruvic acid, citric acid, ferulic acid, cinnamic acid, maleic acid, aconitic acid, benzoic acid, 2-oxoglutarate, succinic acid, fumarate, quinic acid, glucose, fructose, sucrose, sorbitol, myo-inositol, linoleic acid, α-linolenic acid, L-carnitine-d_3, fructose-$^{13}C_6$ and aspartic acid-2,3,3-d_3 were purchased from Sigma-Aldrich. Genistein-d_4, L-proline-2,5,5-d_3, and arachidonic acid-d_5 were obtained from Cayman Chemical Company (Ann Arbor, MI, USA). For the volatile analysis, hexanal, β-pinene, ethyl-2-butenoate, limonene, 3-methylbutan-1-ol, hexen-2-al, γ-terpinene, sulcatone, hexan-1-ol, (*Z*)-3-hexen-1-ol, nonanal, (*E*)-octen-2-al, 2-ethyl-hexan-1-ol, (*E*)-nonen-2-al, linalool, octan-1-ol, *cis*-bergamotene, β-caryophyllene, terpinen-4-ol, nonan-1-ol, L-α-terpienol, and methyl salicylate were purchased from Sigma-Aldrich. 2-Pentylfuran and methyl benzoate were obtained from Santa Cruz Biotechnology.

2.2. Sample preparation

Four cultivars were selected to represent the diversity within U.S. pomegranate production, with 'Wonderful' being the dominant cultivar and 'Azadi', 'Phoenicia', and 'Eversweet' offering variation in acidity and peel color.[12] Additionally, 'Azadi' was included due to its strong reported resistance to anthracnose fruit rot disease, highlighting its agricultural importance.[13] Ten intact fruit from four pomegranate cultivars were sourced from the United States Department of Agriculture, Agricultural Research Service National Clonal Germplasm for Tree Fruit, Nut Crops, and Grapes located in Winters, CA in the United States of America. The fruit were randomly harvested from the mature trees in the germplasm collection during the same season. The fruit from these cultivars were harvested at maturity from multiple trees and were harvested within the same planting block of the other samples; all trees from all cultivars evaluated were planted in the same location in proximity to each other, with no changes in soil type, fertilization, irrigation, nor climate across the growing conditions at this single site. The cultural practices that were used to manage these trees were the same across all cultivars. Samples were knife-scored and pulled apart to obtain intact arils. After weighing all arils, approximately 200 per fruit were placed in a clean Ziploc bag (Ziploc sandwich bag, 6 1/2 in × 5 7/8 in (16.5 cm × 14.9 cm)). The bag was sealed, and the arils were manually pressed to express juice. Once the juice was extracted, it was immediately transferred from the bag into pre-labeled 50 mL conical tubes. The tubes containing 25 mL of juice were placed on ice and then stored at −80 °C for later analysis. Ten biological replicates were prepared for each pomegranate cultivar to ensure statistical reliability. For each chemical analysis, an extraction blank was also prepared by following the corresponding extraction procedure without biological material. The sample analysis sequence was randomized. Quality control (QC) samples were prepared by combining aliquots of all biological samples. To monitor and correct for instrumental drift, QC samples were injected every five samples, and the Pierce FlexMix calibration solution (Thermo Scientific, San Jose, CA, USA) was used for mass calibration throughout the run.

2.3. Anthocyanin quantification

Pomegranate juice was freeze dried using lyophilizer. 100 mg of sample was extracted with 1.0 mL of methanol/water/37%-HCl (50/35/15, V/V/V) with 10 μL butylated hydroxytoluene (BHT, 10 mg mL^{-1}) by sonication for 2 h in an ice-cooled bath. Twenty μL of 10 μg mL^{-1} genistein-d_4 was added as an internal standard. Each mixture was vortexed for 30 min and then centrifuged at 20 000×*g* for 10 min. The supernatants were filtered using 0.2 μm nylon filter prior to LC analysis. The LC-MS/MS system included an Ultimate 3000 UHPLC connected to a triple quadrupole mass spectrometer (TSQ Quantiva, Thermo Fisher Scientific, Waltham, MA, USA). The compounds were eluted through a Waters Acquity CSH C18 column (2.1 mm × 150 mm, 1.7 μm) at 40 °C. A binary eluent consisting of 0.1% formic acid in water (solvent A) and 0.1% formic acid in acetonitrile (solvent B) was used. The gradient system was as follows: 0–22 min 2–60% B, 22.1–28 min 60–100% B, and 28–33 min 100% B, followed by a 5 min re-equilibration at the initial conditions. A flow rate of 0.4 mL min^{-1} was used, with an injection volume set at 4 μL. An electrospray ionization (ESI) interface in positive ion mode was utilized by the mass spectrometer, with ESI settings of a 3500 V spray voltage, an ion transfer tube temperature at 325 °C, vaporizer temperature at 275 °C, and sheath, auxiliary, and sweep gas flows set to 35, 10, and 1 Arb, respectively. MS/MS detection was conducted in selective reaction monitoring (SRM) mode. The optimal MS^2 parameters for each compound are listed in Table S1.† Xcalibur software (version 3.0) was employed for data processing and managing the instrument.

2.4. GC-MS analysis

Solid phase microextraction (SPME) was employed to extract volatile compounds. Specifically, 3 g of pomegranate juice were transferred into a 40 mL headspace vial, to which 10 mL of deionized water containing 0.3 g of sodium chloride was added. Naphthalene-d_8 served as the internal standard. Samples were agitated at 50 °C for 30 min followed by exposure to the divinylbenzene/carboxen/polydimethyl-siloxane SPME fiber for another 30 min. This fiber features 50/30 μm film thickness. The GC-MS analysis was performed using a Thermo Scientific Trace GC 1610 connected to a Thermo TSQ 9610 MS system. A FFAP column (30 m × 0.25 mm × 0.25 μm, Thermo Fisher Scientific) was used to separate volatile compounds (Fig. S1†). Helium served as the carrier gas at a flow rate of 1 mL min^{-1}. A 1.0 μL sample was injected into the GC-MS system for analysis in a splitless mode with the injector at 250 °C. The oven temperature started at 45 °C for 1 minute, then ramped up to 230 °C at 4 °C min^{-1}, holding for 10 minutes. Electron ionization (EI) at 70 eV was employed, with ion source and transmission line temperatures set to 280 °C. Full scan mode detected ions from mass-to-charge ratio (*m*/*z*) 45 to 350. Volatile compounds were identified by matching mass spectra to the NIST library and retention indices (RI), with authenticated standards and linear RIs determined using *n*-alkanes (C7–C30). The peak area ratio of each compound to the internal standard was used to determine its relative content.

2.5. Targeted metabolomics

A targeted metabolomics approach was applied to profile amino acids, organic acids, plant hormones, sugars, and flavonoids. The pomegranate juice sample was freeze-dried using lyophilizer with 0.1 mbar. Seventy milligrams of sample was added with a 0.7 mL of solution (acetonitrile/methanol/water (40/40/20, V/V/V)) and 10 μL of an internal standard mixture (L-carnitine-d_3 ($C_7H_{12}D_3NO_3$), genistein-d_4 ($C_{15}H_6D_4O_5$), aspartic acid-2,3,3-d_3 ($C_4H_4D_3NO_4$), fructose-$^{13}C_6$ ($^{13}C_6H_{12}O_6$), and L-proline-2,5,5-d_3 ($C_5H_6D_3NO_2$)) was added. The Q Exactive Plus mass spectrometer (Thermo Fisher Scientific) was coupled to the Vanquish UHPLC system (Thermo Vanquish Flex Binary RSLC platform). For the reverse phase (RP) system, Thermo Acclaim C30 column (2.1 mm × 150 mm, 3.0 μm) was employed with a mobile phase consisting of 0.1% formic acid in water (eluent A) and 0.1% formic acid in acetonitrile (eluent B). The gradient elution program was as follows: 0 min, 2% B; 3 min, 2%; 25 min 50% B; 30 min 90% B; 30.1 min 95% B; 35 min, 95% B; 35.1 min 2% B; 45 min, 2% B. The flow rate was 0.3 mL min^{-1}, and injection volume was 3 μL (Fig. S2†). For the hydrophilic interaction liquid chromatography (HILIC) system, Agilent Poroshell HILIC-Z column (2.1 mm × 150 mm, 2.7 μm) was employed. Mobile phase consists of eluent A (10 mM ammonium acetate in water) and eluent B (10 mM ammonium acetate in water-acetonitrile (10 : 90, V/V)). The gradient elution program was as follows: 0 min, 90% B; 2 min, 90% B; 15 min, 51% B; 20 min, 51% B; 21 min, 90% B; 30 min, 90% B. The flow rate was 0.25 mL min^{-1}, and injection volume was 3 μL. Both RP and HILIC analyses was performed at 40 °C (Fig. S3†). The t-SIM data were captured with a resolving power of 70,000 (at *m*/*z* 200, full width at half maximum; FWHM). The detailed MS parameters are described in Table S2.† Data were processed with Trace Finder version 4.1 (Thermo Fisher Scientific), identifying and aligning each peak with the standard compounds. The relative quantities were determined by comparing peak areas to an internal standard: organic acids were referenced to L-carnitine-d_3, linear amino acids to aspartic acid-2,3,3-d_3, non-linear amino acids to L-proline-2,5,5-d_3, sugars to fructose-$^{13}C_6$ and plant hormones and flavonoids to genistein-d_4.

For fatty acid analysis, 15 mL of samples were sonicated with 300 mL of chloroform: methanol (2 : 1, V/V) mixture. Arachidonic acid-d_5 was used as an internal standard. After extraction, the sample was concentrated using rotary evaporator, it was dissolved in ethanol and methanol (1 : 1, V/V) mixture to transfer into a 20 mL glass vial. Then the glass vial was evaporated using pure nitrogen. During the evaporation process, 2.5 mg mL^{-1} of butylated hydroxytoluene (BHT) was added to serve as an antioxidant. The fatty acids were redissolved in 400 μL of ethanol and methanol (1 : 1, V/V) mixture and filtered using a nylon syringe filter (0.22 μm), followed by an aliquot injection for LC-MS analysis. The Q Exactive Plus mass spectrometer (Thermo Fisher Scientific, Waltham, MA, USA) coupled with Vanquish UHPLC (Thermo Vanquish Flex Binary RSLC platform) was utilized. A nonpolar gradient system was applied. A Phenomenex Gemini C18 column (2.1 mm × 150 mm, 3.0 μm) was employed with the mobile phase comprising

0.1% formic acid in water as eluent A and 0.1% formic acid in acetonitrile as eluent B. The solvent system was as follows: 0 min 10% B; 3 min, 10% B; 5 min, 60% B; 15 min, 95% B; 20 min, 100% B; 28 min, 100% B. A flow rate of 0.3 mL min^{-1} was used, with an injection volume set at 4 μL. Detailed MS parameters are listed in Table S3.† Data were processed with Trace Finder version 4.1 (Thermo Fisher Scientific). The relative concentration of each compound was calculated based on the ratio of its peak area to that of the internal standard.

All metabolic data were collected and normalized, then MetaboAnalyst 5.0 was used to generate the heatmap and volcano plot.

2.6. Punicalagin analysis

Samples were prepared using the same method for targeted metabolomics and genistein-d_4 was used as an internal standard. SRM mode was employed using an UHPLC system integrated with a triple quadrupole mass spectrometer (TSQ Quantiva, Thermo Fisher Scientific). Punicalagin α and β were separated using an Agilent Acclaim C30 column (2.1 mm × 150 mm, 3.0 μm) at 30 °C (Fig. S4†). Solvent system comprised eluent A (water with 0.1% formic acid) and eluent B (acetonitrile with 0.1% formic acid). The solvent system was as follows: 0 min, 2%; 4 min, 2% B; 18 min 80% B, 19 min, 100% B; 26 min, 100% B. Four microliters of sample were injected, and the system maintained a flow rate of 0.2 mL min^{-1}. The mass spectrometer utilized an ESI interface and was operated in the negative ionization mode. Detailed MS setting and optimized precursor and product ion information is described in Tables S4 and S5.† The relative concentration was quantified by calculating the ratio of its peak area to the peak area of the internal standard.

3. Results & discussion

3.1. Volatile compounds

A total of 27 volatile compounds were determined from pomegranate juice. These include seven aldehydes (hexanal, hexen-2-al, nonanal, (*E*)-octen-2-al, (*E*)-nonen-2-al, *p*-tolualdehyde, 2,4-dimethylbenzaldehyde), six alcohols (hexan-1-ol, (*Z*)-3-hexen-1-ol, 2-ethyl-hexan-1-ol, octan-1-ol, nonan-1-ol, 3-methyl-butan-1-ol), seven monoterpenes (β-pinene, limonene, γ-terpinene, *o*-cymene, linalool, L-α-terpineol, terpinen-4-ol), three esters (methyl benzoate, methyl salicylate, ethyl-2-butenoate), two sesquiterpenes (*cis*-bergamotene, β-caryophyllene), one furan (2-pentylfuran), and one ketone (sulcatone). Among them, 25 compounds were fully confirmed using the authentic standards and the remaining 2 compounds were tentatively identified by RI and MS. The relative abundance of each volatile was listed in Table 1 and their chemical properties were detailed in Table

Table 1 Relative abundance of volatile compounds in pomegranate juice[a]

No.	Volatiles	RT (min)	RI[b]	Azadi	Eversweet	Phoenicia	Wonderful
1	Hexanal[c]	4.89	1064	0.37 ± 0.08	0.21 ± 0.04	0.32 ± 0.08	0.46 ± 0.10
2	β-Pinene[c]	6.21	1138	0.49 ± 0.03	0.32 ± 0.01	0.86 ± 0.18	1.06 ± 0.22
3	Ethyl-2-butenoate[c]	6.65	1158	0.06 ± 0.02	0.00 ± 0.00	0.00 ± 0.00	0.00 ± 0.00
4	Limonene[c]	6.85	1166	0.04 ± 0.01	7.76 ± 2.21	0.05 ± 0.02	10.19 ± 2.67
5	3-Methyl-1-butanol[c]	7.92	1211	0.11 ± 0.02	0.00 ± 0.00	0.06 ± 0.02	0.05 ± 0.01
6	2-Hexenal[c]	8.02	1215	0.64 ± 0.14	0.91 ± 0.20	0.28 ± 0.06	0.59 ± 0.14
7	2-Pentylfuran[c]	8.21	1222	0.11 ± 0.03	0.06 ± 0.02	0.15 ± 0.04	0.55 ± 0.17
8	γ-Terpinene[c]	8.51	1232	0.04 ± 0.01	0.05 ± 0.02	1.78 ± 0.32	0.15 ± 0.03
9	*o*-Cymene[d]	9.10	1254	0.28 ± 0.06	0.25 ± 0.06	1.06 ± 0.22	0.58 ± 0.11
10	Sulcatone[c]	11.40	1335	1.26 ± 0.27	1.49 ± 0.38	0.23 ± 0.05	0.29 ± 0.05
11	1-Hexanol[c]	11.93	1353	19.02 ± 1.22	19.53 ± 3.46	22.24 ± 3.02	28.05 ± 4.77
12	(*Z*)-3-Hexen-1-ol[c]	12.86	1385	9.92 ± 1.52	7.24 ± 1.58	9.76 ± 1.31	21.57 ± 3.98
13	Nonanal[c]	13.04	1391	3.15 ± 0.66	0.09 ± 0.02	1.45 ± 0.27	0.24 ± 0.05
14	(*E*)-2-Octenal[c]	14.11	1427	1.79 ± 0.46	0.96 ± 0.18	6.80 ± 1.24	0.74 ± 0.17
15	2-Ethyl-1-hexanol[c]	16.0	1490	3.53 ± 0.82	2.51 ± 0.49	3.97 ± 0.88	1.06 ± 0.18
16	(*E*)-2-Nonenal[c]	17.24	1532	0.16 ± 0.04	0.30 ± 0.09	0.12 ± 0.03	0.25 ± 0.04
17	Linalool[c]	17.69	1548	0.35 ± 0.04	0.05 ± 0.01	0.44 ± 0.11	0.61 ± 0.14
18	1-Octanol[c]	18.03	1559	1.50 ± 0.30	3.03 ± 0.66	0.64 ± 0.13	1.12 ± 0.21
19	*cis*-Bergamotene[d]	18.44	1573	0.10 ± 0.02	0.60 ± 0.13	0.10 ± 0.02	0.86 ± 0.16
20	β-Caryophyllene[c]	18.61	1579	0.14 ± 0.04	0.51 ± 0.10	1.06 ± 0.24	0.09 ± 0.02
21	Terpinen-4-ol[c]	19.14	1598	0.68 ± 0.12	0.48 ± 0.10	1.18 ± 0.20	0.86 ± 0.16
22	Methyl benzoate[c]	19.78	1620	0.09 ± 0.02	0.48 ± 0.10	0.71 ± 0.13	0.93 ± 0.17
23	*p*-Tolualdehyde[d]	20.53	1646	1.49 ± 0.36	0.12 ± 0.03	9.02 ± 1.65	5.66 ± 1.28
24	1-Nonanol[c]	20.99	1663	1.58 ± 0.35	0.02 ± 0.00	0.86 ± 0.20	0.59 ± 0.13
25	L-α-Terpineol[c]	21.86	1693	7.10 ± 1.34	6.68 ± 1.26	5.26 ± 1.08	7.24 ± 1.74
26	Methyl salicylate[c]	24.23	1780	0.03 ± 0.01	0.49 ± 0.10	0.65 ± 0.15	0.11 ± 0.02
27	2,4-Dimethylbenzaldehyde[d]	25.0	1809	0.04 ± 0.01	1.17 ± 0.24	1.29 ± 0.25	0.98 ± 0.21

[a] The intensity of each peak was normalized by internal standard. [b] Retention indices were determined on TR-FFAP capillary column using *n*-alkanes C7–C30 as external reference. [c] The reliability of the identification proposal is indicated by the following: mass spectrum and retention index were consistent with those of an authentic standard. [d] The reliability of the identification proposal is indicated by the following: MS, mass spectrum was consistent with that of the NIST library. Values are expressed as means ± standard deviation.

S6.† Overall, hexan-1-ol, (*Z*)-3-hexen-1-ol, L-α-terpineol, and limonene were present in higher concentrations than the other compounds. Compared to non-volatile compounds, significant differences were observed among the groups. For example, ethyl-2-butenoate, first reported in pomegranate, was present only in 'Azadi'. Another newly reported compound, 3-methyl-butan-1-ol, was found only in 'Azadi', 'Phoenicia', and 'Wonderful', but not in 'Eversweet'. Thus, as shown in the volcano plot, compounds on the far left and right are mostly volatile compounds (Fig. S5†).

3.2. Key pathway analysis

To uncover the underlying metabolic pathways associated with the primary metabolites with flavor-related compounds distinctive to pomegranates, the Kyoto encyclopedia of genes and genomes (KEGG) pathway database was consulted along with a comprehensive literature review. This approach led to the identification and selection of four key flavor biosynthetic pathways: the shikimate and phenylpropanoid pathway, terpenoid backbone biosynthesis, lipoxygenase pathway, and citric acid cycle pathway. A pathway-based targeted metabolomics method was employed to investigate the metabolic responses in the selected pathways across the four pomegranate cultivars (Azadi, Eversweet, Phoenicia, and Wonderful). Compounds were mapped onto the pathway, providing a comprehensive view of the metabolic flow, from flavor precursors to intermediates and final products.

3.3. Shikimate and phenylpropanoid pathway

3.3.1. Phenolic volatiles. The shikimate/phenylpropanoid pathway is typically utilized by plants to generate phenolic volatiles as well as non-volatile phenolic compounds. The shikimic acid and phenylpropanoid pathways, located in the plastid and chloroplast, respectively, are interconnected and contribute to the production of a wide range of phenolic compounds, either directly or through related branches.[14] The shikimic acid pathway is vital in higher plants like pomegranate, producing phenylalanine, a key precursor for the phenylpropanoid pathway.[15] Phenylalanine is first converted into *trans*-cinnamic acid by phenylalanine ammonia-lyase, followed by a hydroxylation reaction that transforms *trans*-cinnamic acid into *p*-coumaric acid. Finally, *p*-coumaric acid is converted into *p*-coumaroyl-CoA, a crucial intermediate in phenylpropanoid biosynthesis.[16]

Simultaneously, some cinnamic acid is converted into benzoic acid, followed by the formation of phenolic volatiles such as methyl benzoate and methyl salicylate. The removal of the two-carbon side chain from cinnamic acid (C6–C3 structure) to yield benzoic acid (C6–C1 structure) can occur *via* β-oxidation or a non-β-oxidative pathway.[17] The presence of a phenol group enables a broad and strong affinity for the human olfactory receptor, namely OR10G. This occurs because the benzene ring easily interacts with receptors through π–π electron interactions.[18]

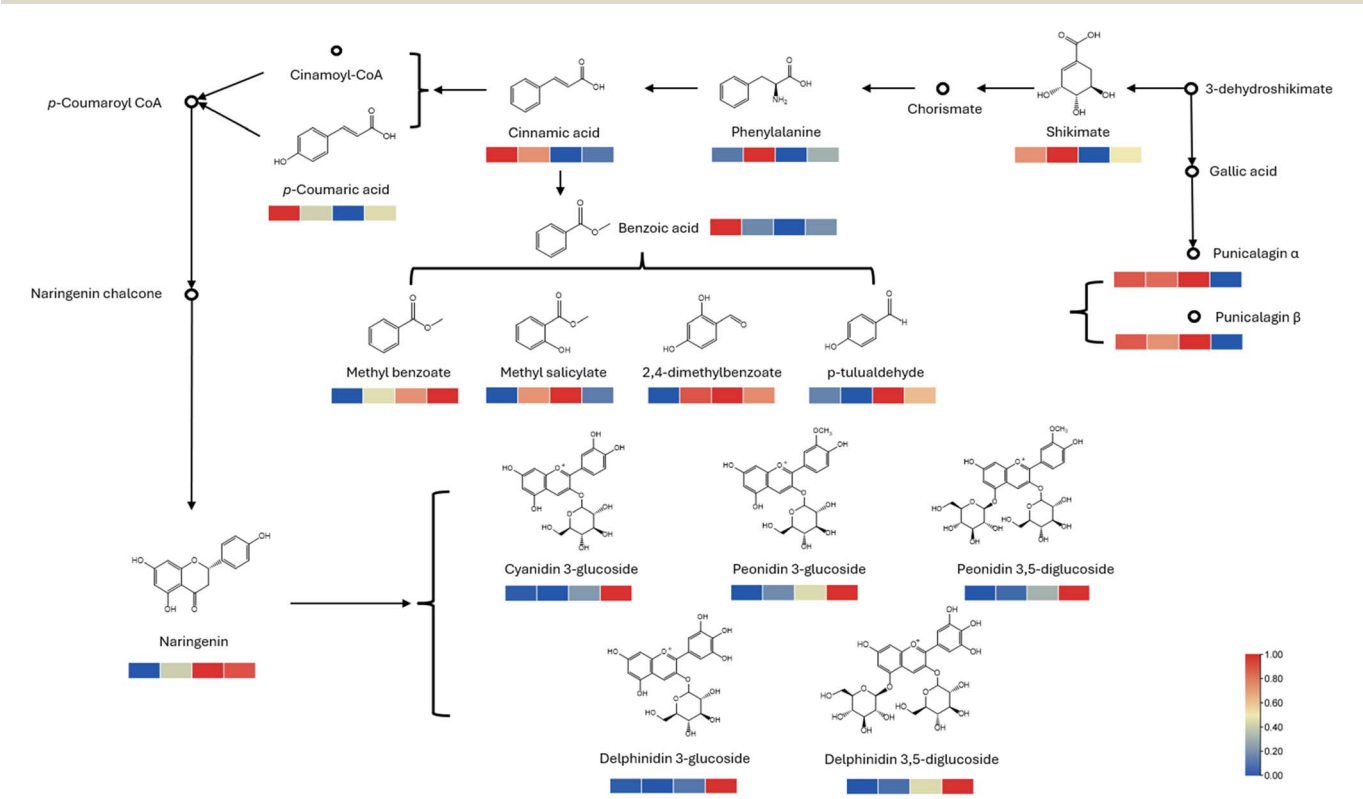

Fig. 1 Metabolite mapping on the shikimate and phenylpropanoid pathways. Each analyzed metabolite is represented by a scale consisting of four grids. The four grids indicate the relative concentrations for each cultivar: Azadi, Eversweet, Phoenicia, and Wonderful, respectively, from left to right.

In our study, as shown in Fig. 1, four benzoic acid derived volatiles were detected, including methyl benzoate, methyl salicylate, 2,4-dimethylbenzoate, and *p*-tolualdehyde. 'Phoenicia' exhibited the highest concentrations in three of these compounds and the second-highest concentration in one volatile, methyl benzoate. Interestingly, despite these high levels, 'Phoenicia' showed the lowest concentrations of their precursors (benzoic acid and cinnamic acid). 'Phoenicia' might actively up-regulate this biosynthetic pathway to rapidly consume the available precursors. In contrast, 'Azadi' showed the lowest concentrations of end products (benzoic acid-derived volatiles), despite having the highest levels of their precursors. 'Azadi' may not have actively up-regulated this pathway to produce benzoic acid-derived volatiles. The two cultivars also showed an analogous opposite trend in their other secondary phenolic compounds. 'Azadi' showed low concentrations of other secondary phenolic compounds, despite its high concentration of coumaric acid, which can serve as a starting metabolite in the phenylpropanoid pathway. However, 'Phoenicia' showed high concentration of naringenin despite its low concentration of coumaric acid. The increase of naringenin in 'Phoenicia' might induce the biosynthesis of downstream anthocyanins.

3.3.2. Anthocyanin quantification. Anthocyanins are pigments commonly found in most vascular plants and are particularly abundant in pomegranates. The hue of anthocyanins depends on the functional groups like hydroxyl and methyl. Hydroxylation on the B-ring of anthocyanins enhances the pigment's blue coloration. This is because the added hydroxyl groups increase the electron-donating capacity, which stabilizes the anthocyanin structure, favoring its blue form. Conversely, methylation of the hydroxyl groups on the B-ring induces a red shift in the pigment (Fig. S6†). This occurs because methyl groups reduce the electron-donating effect, leading to a less stable structure, shifting the color towards red.[19,20] The glucosylated forms of cyanidin, delphinidin, and peonidin are the most prevalent anthocyanins found in pomegranate. Cyanidin has two hydroxyl groups on the B-ring (at positions 3′ and 4′), while delphinidin has three hydroxyl groups (at positions 3′, 4′, and 5′). The additional hydroxyl group in delphinidin contributes to a shift toward a bluer color compared to cyanidin. Meanwhile, peonidin is a methylated derivative of cyanidin, where the methylation of the hydroxyl group at the 3′ position of the B-ring leads to a shift in color towards red. Beyond aglycon modifications, glycosylation of anthocyanins significantly contributes to fruit color. C3 glycosylation is prevalent among naturally occurring anthocyanins, primarily involving the addition of glucose *via* UDP-3-*O*-glucosyltransferases (UFGT/3GT). This process results in a red shift. Additionally, C3 biosides are more stable than their monoglycoside counterparts, which is why 3,5-diglycosides are also commonly found in the plant kingdom.[21,22]

In our study, the concentrations of eight anthocyanins (cyanidin 3-glucoside, cyanidin 3,5-diglucoside, cyanidin 3-rutinoside, delphinidin 3-glucoside, delphinidin 3,5-diglucoside, delphinidin 3-rutinoside, peonidin 3-glucoside, and peonidin 3,5-diglucoside) were quantified using triple quadrupole mass spectrometry with standard compounds. Retention times varied between 4.91 and 7.45 minutes, with clear separation of analytes and no observed interference. The elution order of the detected anthocyanins was consistent with previously reported literature.[23] For eight anthocyanins, calibration samples were prepared at six concentration levels, ranging between 0.01 and 1000 μg mL^{-1}. Calibration curves, based on the peak area ratios relative to the internal standard (genistein-d_4), exhibited linearity with r^2 values greater than 0.9995. Limits of detection (LOD) and quantification (LOQ) were determined at S/N ratios of 3.3 and 10, respectively. The LODs and LOQs were 0.01–0.031 μg mL^{-1} and 0.033–0.095 μg mL^{-1}, respectively (Table S7†). Precision and accuracy were determined as well (Table S8†).

As shown in Table 2, delphinidin 3,5-diglucoside, delphinidin 3-glucoside, cyanidin 3,5-diglucoside, and cyanidin 3-glucoside are the primary anthocyanins. 'Wonderful' exhibited the highest concentrations of seven anthocyanins, with the exception of delphinidin 3-rutinoside. Additionally, cyanidin 3-rutinoside was exclusively detected in 'Wonderful'. 'Phoenicia' showed the second highest concentrations followed by 'Azadi' and 'Eversweet'. The elevated anthocyanin concentration in 'Wonderful' likely accounts for its deeper red color compared to the other three cultivars. The elevation of the upstream metabolite (naringenin) in 'Wonderful' and 'Phoenicia' aligns with the downstream metabolite (anthocyanins). Previous

Table 2 Concentrations of anthocyanins in pomegranate juice

		Concentration (mg kg^{-1})			
No.	Anthocyanin	Azadi	Eversweet	Phoenicia	Wonderful
1	Cyanidin 3,5-diglucoside	55.19 ± 7.11[a]	131.72 ± 15.45	481.8 ± 60.87	830.45 ± 144.44
2	Cyanidin 3-glucoside	75.91 ± 9.45	68.23 ± 7.58	158.34 ± 18.12	461.45 ± 50.4
3	Cyanidin 3-rutinoside	—	—	—	0.92 ± 0.09
4	Delphinidin 3,5-diglucoside	46.94 ± 5.44	121.86 ± 11.62	429.36 ± 47.67	893.84 ± 121.51
5	Delphinidin 3-glucoside	28.79 ± 3.8	24.23 ± 3.0	47.19 ± 6.14	240.57 ± 23.06
6	Delphinidin 3-rutinoside	0.45 ± 0.01	0.36 ± 0.04	0.38 ± 0.01	0.42 ± 0.01
7	Peonidin 3,5-diglucoside	2.81 ± 0.4	7.84 ± 0.98	26.48 ± 3.35	78.98 ± 8.92
8	Peonidin 3-glucoside	7.86 ± 0.96	13.97 ± 1.89	23.3 ± 3.25	42.12 ± 3.89

[a] Data are expressed as means ± standard deviation. Means were calculated from ten biological replicates per cultivar.

studies have also identified 'Wonderful' as the cultivar with the highest anthocyanin content.[23] This result indicates that 'Wonderful' may exhibit a stronger antioxidant effect due to its high anthocyanin content, which is known for various bioactivities, including anti-inflammatory, antioxidant, anticancer, and neuroprotective effects.[6]

3.3.3. Punicalagin analysis. Alongside anthocyanins, punicalagin is another distinctive compound found in pomegranate, and it is rarely present in other fruits.[24] It is plentiful in pomegranate juice, fruit, peel (pericarp), seeds, flowers, leaves, and bark. The synthesis of punicalagin, a major derivative of gallic acid, occurs through a series of enzymatic processes, including galloyl group transfer and the formation of glucose esters. This pathway suggests that punicalagin is derived from 3-dehydroshikimate, which aids in converting gallic acid into more complex compounds like ellagic acid, eventually leading to punicalagin formation.[25] In pomegranate, two isomeric forms of punicalagin are biosynthesized, namely punicalagin

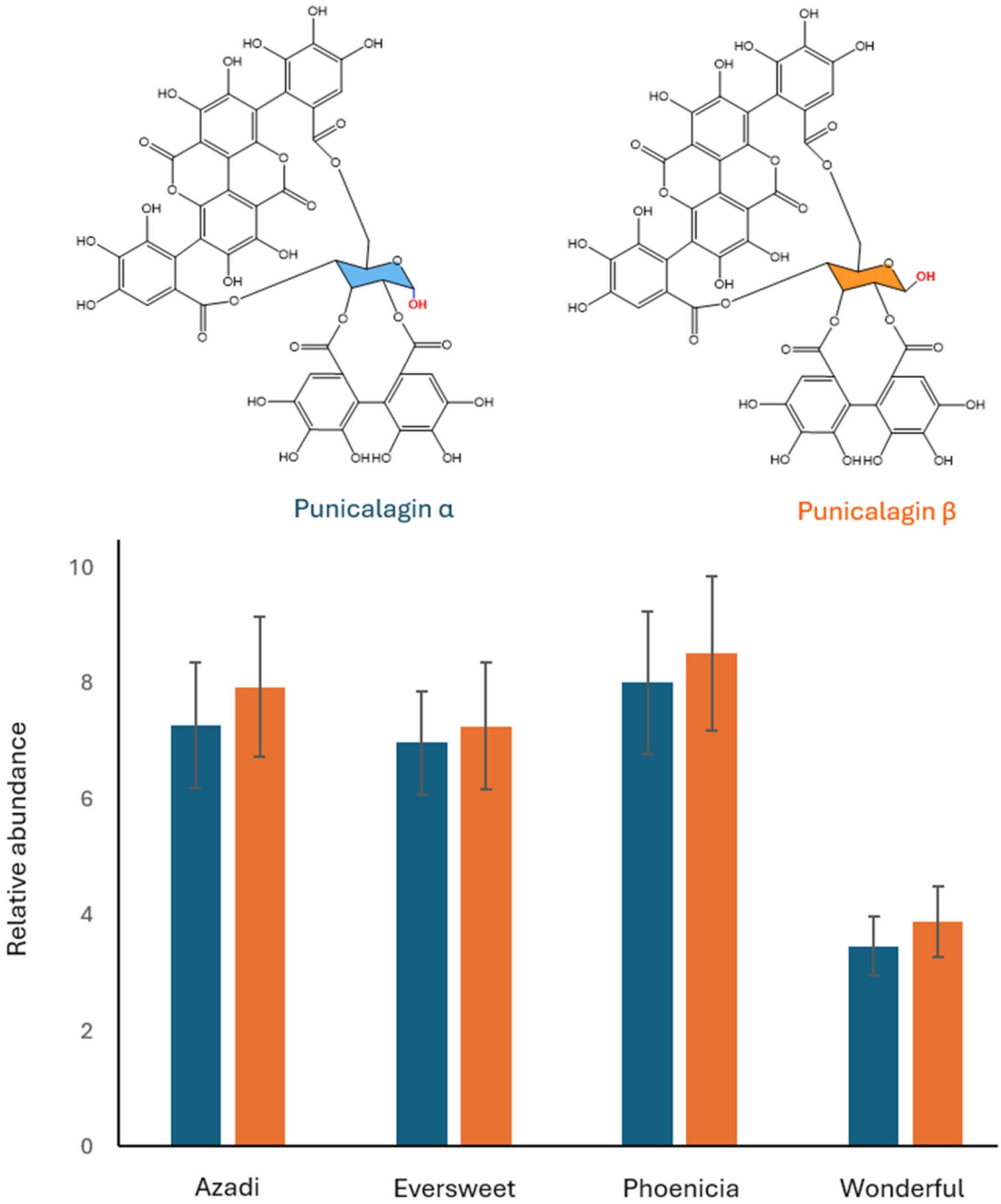

Fig. 2 Relative abundance of Punicalagin α and β and their chemical structure. The left bar indicates the relative abundance of punicalagin α and the right bar indicates that of punicalagin β. Values are mean ± SD ($n = 10$).

α and β. The structural feature of punicalagin is that it consists of a glucose core linked to both galloyl groups and hexahydroxydiphenoyl (HHDP) groups. The configuration of this core glucose determines whether it is α or β punicalagin.[26] Upon administration, punicalagin is metabolized by colonic microflora into bioavailable hydroxy-6*H*-dibenzopyran-6-one derivatives, known as urolithins. Urolithins are well-documented for their health benefits, including anticancer, cardiovascular protective, and antioxidant effects.[27]

In this study, punicalagin α and β were semi-quantified using a standard reagent. Fig. S4† illustrates the peak of each compound along with their corresponding structures. Among the cultivars, 'Phoenicia' exhibited the highest amount, followed by 'Azadi', 'Eversweet', and 'Wonderful' (Fig. 2). The ratio of punicalagin α to punicalagin β was similar across all four cultivars, ranging from 0.90 to 0.96 (Table S9†). This could be because they are formed through the same biosynthetic pathway, differing only in the stereochemistry of the glucose configuration.

3.4. Terpenoid backbone

Terpenoids are synthesized from the five-carbon building blocks, isopentenyl diphosphate (IPP) and its isomer dimethylallyl diphosphate (DMAPP), which are produced by two distinct but interacting pathways: the mevalonic acid (MVA) pathway and the methylerythritol phosphate (MEP) pathway. In plants, these pathways are compartmentally separated, with the MVA pathway occurring in the cytosol and peroxisomes, and the MEP pathway in plastids.[28] This separation leads to the MEP pathway being primarily responsible for the generation of monoterpenes, while the MVA pathway predominantly produces sesquiterpenes. However, despite their separation, there is metabolic crosstalk between the two pathways through the exchange of intermediates like IPP, allowing both pathways to contribute to terpene synthesis under certain conditions.[29]

In our study, seven monoterpenes (β-pinene, limonene, linalool, L-α-terpineol, γ-terpinene, terpinen-4-ol, *o*-cymene) and two sesquiterpenes (*cis*-bergamotene, caryophyllene) were detected. The increased upstream metabolites (pyruvic acid) in MEP pathway could be attributed to the elevated concentration of downstream monoterpenes in 'Wonderful'. Meanwhile, an elevated upstream metabolite (mevalonate) in the mevalonate pathway increased downstream sesquiterpenes in 'Phoenicia' and 'Wonderful' (Fig. 3).

'Wonderful' showed the highest concentration for four monoterpenes (β-pinene, limonene, linalool, and L-α-terpineol) and one sesquiterpene (*cis*-bergamotene). 'Phoenicia' showed the highest concentration for three monoterpenes (γ-terpinene, terpinen-4-ol, *o*-cymene) and one sesquiterpene (caryophyllene). Overall, 'Phoenicia' produced more cyclic and bicyclic terpenes than other cultivars. 'Azadi' and 'Eversweet' showed lower concentrations of terpenes. Interestingly, terpenes abundant in 'Phoenicia' are well known for their antimicrobial and antioxidant activities. Terpinen-4-ol, for example, has been reported to combat pathogens in *Candida* species, grape, wheat grain, and more.[30–32] Moreover, terpinen-4-ol has also been shown to enhance the expression of genes involved in JA synthesis, such as FaLOX, FaAOC, and FaOPR3 to improve disease resistance.[33] The increased level of terpinen-4-ol might have contributed to the elevated levels of JA and JA-Ile in 'Phoenicia' in our study. Caryophyllene, which was found in the highest concentration in 'Phoenicia', has also been shown to enhance pathogen resistance in diverse plants such as maize, rice, and zucchini, acting as a primary defense volatile.[34,35]

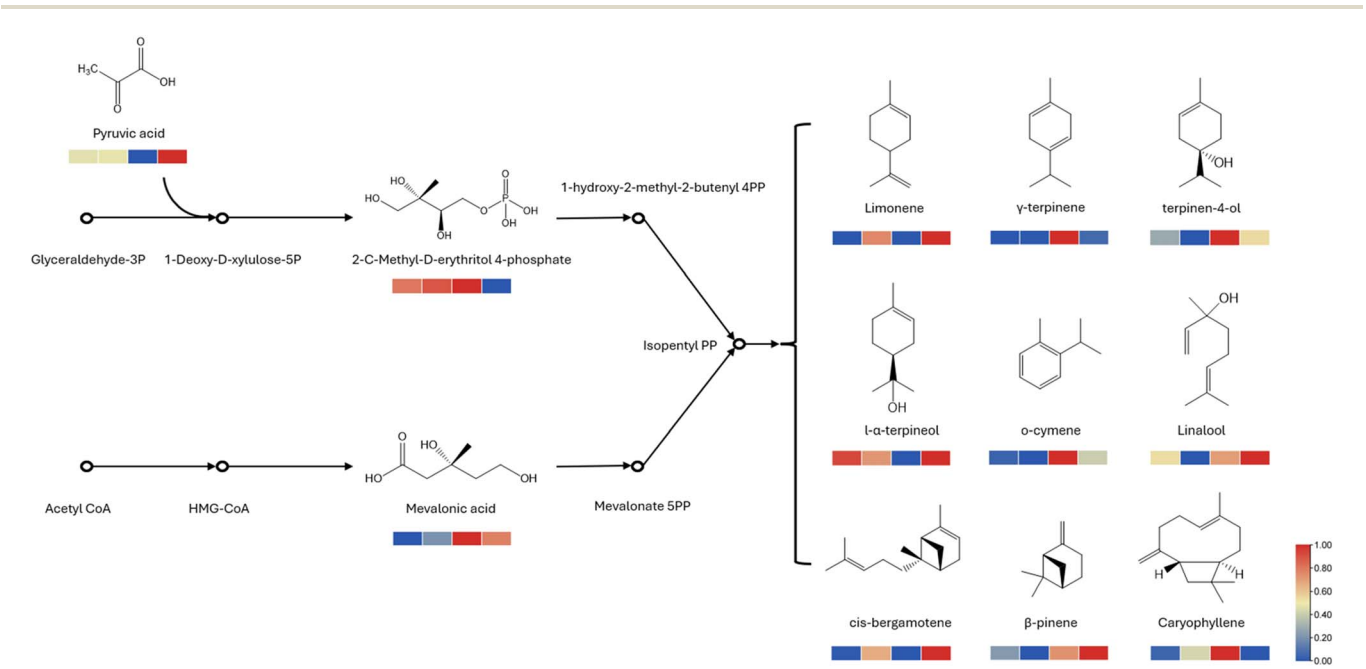

Fig. 3 Metabolite mapping on the terpene backbone pathway. Each analyzed metabolite is represented by a scale consisting of four grids. The four grids indicate the relative concentrations for each cultivar: Azadi, Eversweet, Phoenicia, and Wonderful, respectively, from left to right.

On the other hand, 'Wonderful' tends to produce more terpenes that are well recognized for their role in pollinator attraction and distinctive aromatic profiles. Linalool has been documented to attract pollinators, including fig wasps, fungus gnats, and moths, in plants like *Ficus hispida*, *Mitella*, and *Datura wrightii*.[36,37] Limonene is also known to attract pollinators in various plants, including *Stevia rebaudiana*, monkey flower, and lucerne flowers.[38–40] This increased production of pollinator-attracting volatiles in 'Wonderful' may be an adaptive response to enhance reproductive success. In pomegranates cultivars with more typical floral development (*e.g.*, 'Eversweet', 'Phoenicia'), the percentage of male flowers generally ranges from 45.2% and 72.8%, allowing for a higher proportion of hermaphroditic flowers capable of setting fruit. In contrast, 'Wonderful' exhibits approximately 93% staminate (male) flowers, which have little capacity to produce fruit.[41] This high proportion of staminate flowers presents a significant reproductive limitation. Thus, by producing higher levels of pollinator-attracting compounds, 'Wonderful' might be compensating for the reproductive limitation. So far, no research has been conducted to elucidate the volatile compounds in 'Wonderful' and its pollinator. Further study is necessary to elucidate this mechanism.

3.5. LOX pathway

Lipoxygenases (LOXs) are important enzymes in plants that oxygenate polyunsaturated fatty acids (PUFAs) such as linoleic acid and α-linolenic acid. They introduce oxygen at designated sites on the fatty acid chain, leading to the formation of hydroperoxyl fatty acids. This oxygenation can take place at distinct carbon positions on the PUFA chain, primarily mediated by two types of LOX enzymes: 13-LOX and 9-LOX.[42] 13-lipoxygenase (13-LOX) enzymes are designed to specifically oxygenate linoleic acid or α-linolenic acid at the 13th carbon position. The enzyme's active site structure dictates this specificity, with the fatty acid substrate entering the pocket with its methyl end first. With this orientation, hydrogen is selectively removed from the C-11 position, allowing for oxygen to be inserted at the C-13 position.[43] This process generates 13*S*-hydroperoxyoctadecadienoic acid (13*S*-HPODE), which then leads to the formation of C6 volatiles. C6 volatile compounds are important for the characteristic "green" aroma in many fruits and vegetables.

In our study, as shown in Fig. 4, four C6 volatile compounds, including hexanal, hexen-2-al, hexan-1-ol, and *trans*-3-hexen-1-ol were detected. 'Wonderful' had the highest levels of the three C6 volatiles, except for hexen-2-al, with 'Azadi' following behind. Notably, 'Wonderful' showed lower levels of their precursors, such as linoleic acid, linolenic acid, and 13-HPODE. 'Wonderful' might up-regulate this pathway to consume its available precursors.

9-Lipoxygenase (9-LOX) enzymes specifically target the 9th carbon of the fatty acid substrate for oxygenation. Unlike 13-LOX, the substrate enters the active site with the carboxyl end leading. This inverted orientation removes hydrogen from the C-8 position, allowing for oxygen insertion at the C-9 position. This process generates 9*S*-hydroperoxyoctadecadienoic acid (9*S*-

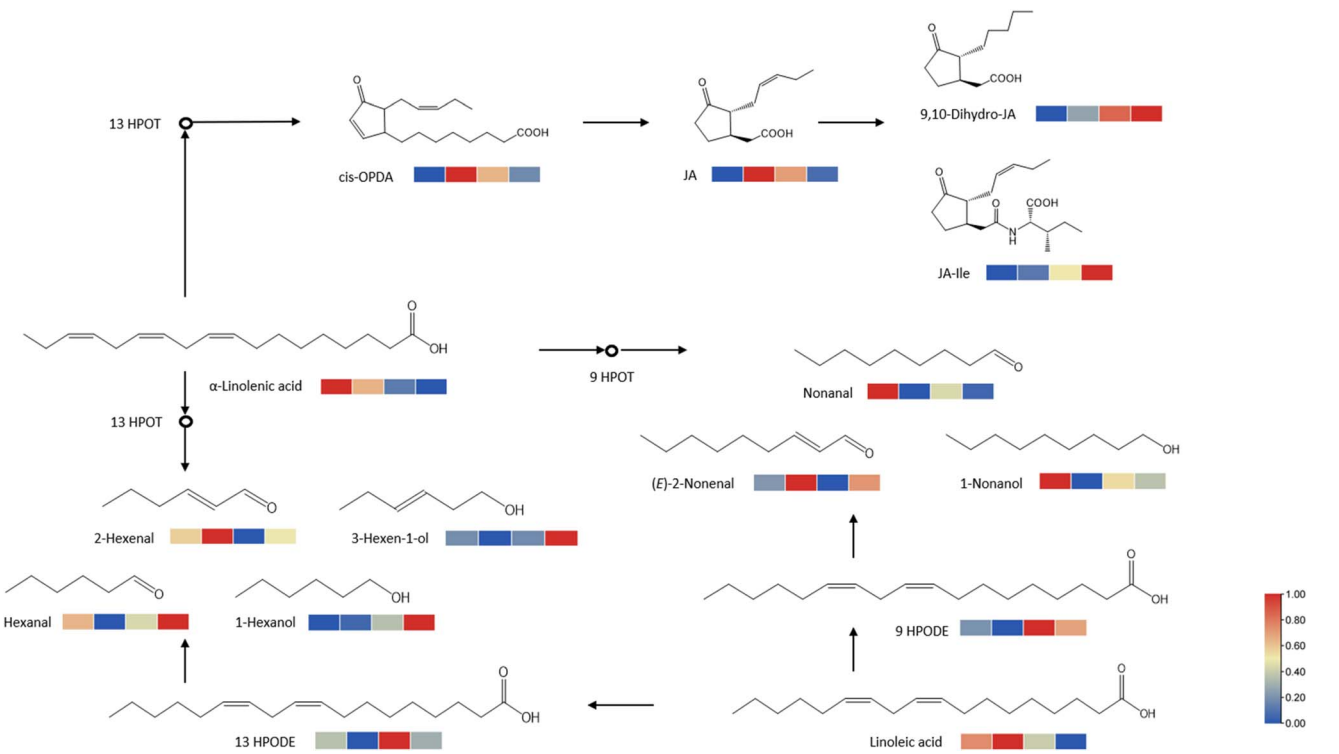

Fig. 4 Metabolite mapping on the lipoxygenase pathway. Each analyzed metabolite is represented by a scale consisting of four grids. The four grids indicate the relative concentrations for each cultivar: Azadi, Eversweet, Phoenicia, and Wonderful, respectively, from left to right.

HPODE), which then leads to the formation of C9 volatile compounds.[43] In our study, three C9 volatiles were detected. 'Azadi' showed the highest amounts of nonanal and nonan-1-al. 'Azadi' also exhibited higher levels of precursors such as α-linolenic acid and linoleic acid. This pattern contrasts with 'Wonderful', which shows high levels of C6 volatiles but low levels of their precursors. 9-LOX pathway in 'Azadi' might be moderately up-regulated, allowing for the accumulation of C9 volatiles without rapidly depleting the precursor fatty acids.

"alpha"-Linolenic acid can serve as a precursor of jasmonic acid as well. It is first converted into 13-HPOT, which is then transformed into *cis*-(+)-12-oxo-phytodienoic acid (OPDA), a direct precursor of JA in plastids and peroxisomes. Jasmonic acid plays a vital role in the signaling network that regulates growth, stress responses, and defenses against herbivores and pathogens.[44]

Interestingly, although 'Azadi' had the highest levels of α-linolenic acid, a precursor of JA, it exhibited the lowest amounts of JA and its derivatives (9,10-dihydro JA and JA-Ile). As mentioned above, 'Azadi' might maintain a high level of α-linolenic acid to synthesize high amounts of C9 volatiles. On the other hand, 'Wonderful' and 'Phoenicia' showed different behavior from 'Azadi'. 'Wonderful' and 'Phoenicia' had the lowest levels of α-linolenic acid, yet they showed high concentrations of JA derivatives (9,10-dihydro-JA and JA-Ile). JA biosynthesis was highly up-regulated in 'Wonderful' and 'Phoenicia', resulting in the rapid conversion of α-linolenic acid into JA derivatives. 'Wonderful' and 'Phoenicia' may actively employ JAs for various purposes. Additionally, 'Wonderful' and 'Phoenicia' might utilize JA derivatives to enhance fruit quality, such as achieving vivid coloration. Inhibition of JA-Ile by Jarin-1 has been shown to reduce anthocyanin concentration in strawberries.[45] Thus, the high concentration of JA-Ile in 'Wonderful' and 'Phoenicia' could contribute to the elevated anthocyanin levels observed in these two cultivars.

3.6. Citric acid cycle

One of the special features of pomegranate is its sour taste. Pomegranate juice has a pH range from 2.7 to 3.6 and titratable acidity in percent citric acid equivalents (TA) from 0.2 to 2.0%. Citric acid was known as the most abundant sour organic acid in pomegranate, followed by malic acid, succinic, tartaric, oxalic acid.[11] These metabolites are strongly involved in the tricarboxylic acid (TCA) cycle, which serves as a central metabolic pathway that occurs in the mitochondria of plant cells. The cycle initiates with the condensation of acetyl-CoA and oxaloacetate, which is then sequentially transformed into intermediates such as isocitrate, α-ketoglutarate, succinate, fumarate, and malate.[46]

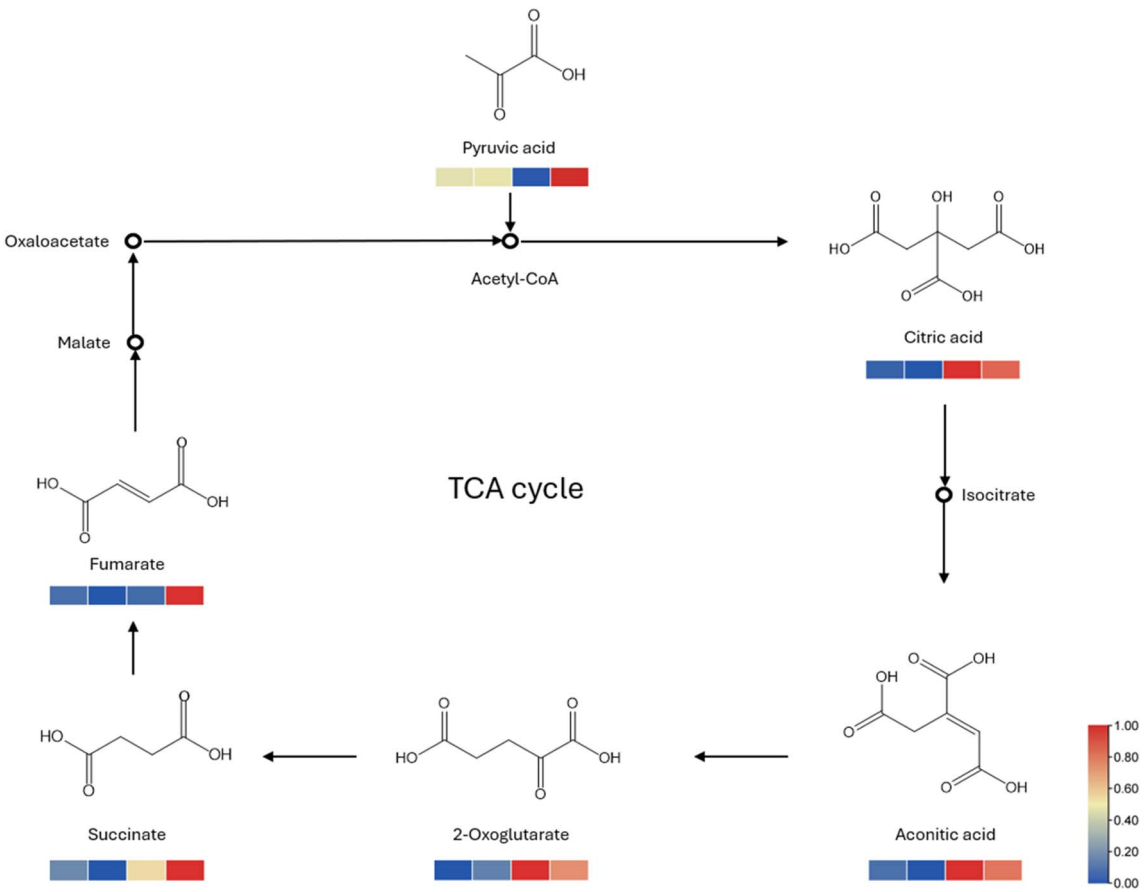

Fig. 5 Metabolite mapping on the citric acid cycle. Each analyzed metabolite is represented by a scale consisting of four grids. The four grids indicate the relative concentrations for each cultivar: Azadi, Eversweet, Phoenicia, and Wonderful, respectively, from left to right.

As shown in Fig. 5, 'Phoenicia' and 'Wonderful' showed significantly higher concentration and 'Azadi' and 'Eversweet' showed low concentration of citric acid. The differences in the accumulation of citric acid and malic acid in different cultivars could indeed be related to their transport mechanisms into the vacuole. In plants, organic acids like citric acid and malic acid are transported into the vacuole *via* specific transporters and channels, and the efficiency and regulation of these transport mechanisms can vary depending on the type of acid and the plant species or cultivar.[47] Some cultivars may have more efficient citrate channels, leading to higher citric acid accumulation, while others may have less efficient malate transporters, resulting in lower malic acid levels. Interestingly, 'Phoenicia' showed the highest amount in citrate and 2-oxoglutarate, while 'Wonderful' showed the highest concentrations of succinate and fumarate. It suggests that 2-oxoglutarate in 'Phoenicia' might be partially diverted towards other pathways such as energy production, amino acid synthesis, fatty acid synthesis, or gamma-aminobutyric acid (GABA) production.

4. Conclusions

In summary, this study explored the biosynthesis of essential flavor-related compounds in pomegranate through a pathway-focused metabolomics approach. Differentially expressed metabolites were screened to profile major flavor pathways, including the shikimate/phenylpropanoid biosynthesis, terpenoid backbone biosynthesis, lipoxygenase pathway, and TCA cycle metabolism. The results demonstrated the flow of metabolites through these pathways and underscored the connections between flavor precursors and their end products. Based on these findings, possible mechanisms for the formation and regulation of key flavor compounds in pomegranate were identified and discussed. Our study provides novel insights into the biosynthesis processes occurring within four California-grown pomegranate cultivars. Notably, 'Wonderful' up-regulated the majority of pathways, leading to increased production of phenolic compounds, terpenes, fatty acids, and JA derivatives. While this may enhance its antioxidant properties, it could also result in a more bitter taste, potentially reducing consumer preference. Since 'Wonderful' is the dominant cultivar in California, further research, particularly focusing on gene expression and phylogenetic analysis, is necessary to fully understand these biosynthetic processes and their impact on flavor development.

Data availability

The data supporting this article have been included as part of the ESI.†

Author contributions

Jin-Pyo An: writing – original draft, investigation, formal analysis. Dongjoo Kim: data curation. Xuebo Song: validation. John M. Chater: methodology, conceptualization. Claire C. Heinitz: resources. Yu Wang: writing – review and editing, supervision, project administration.

Conflicts of interest

There are no conflicts to declare.

Acknowledgements

This project was supported by the USDA Agricultural Marketing Service (AMS) MultiState Specialty Crop Block Grant through the California Department of Food and Agriculture project number 19-1043-002-SF.

References

1 H. A. Asadi-Gharneh, M. Mohammadzamani and S. Karimi, *Int. J. Fruit Sci.*, 2017, **17**, 175–187.
2 N. M. Hegazi, S. El-Shamy, H. Fahmy and M. A. Farag, *J. Food Compos. Anal.*, 2021, **97**, 103773.
3 L. Pienaar and V. Barends-Jones, *Agriprobe*, 2021, **18**, 57–64.
4 AGMRC, Pomegranate, retrieved from, **https://www.agmrc.org/commodities-products/fruits/pomegranates/**, accessed January 14, 2025.
5 J. M. Bueno, P. Sáez-Plaza, F. Ramos-Escudero, A. M. Jiménez, R. Fett and A. G. Asuero, *Crit. Rev. Anal. Chem.*, 2012, **42**, 126–151.
6 E. Pojer, F. Mattivi, D. Johnson and C. S. Stockley, *Compr. Rev. Food Sci. Food Saf.*, 2013, **12**, 483–508.
7 E. Marcano, *Energy Harvest. Syst.*, 2018, **5**, 29–38.
8 B. Tang, Y. He, J. Liu, J. Zhang, J. Li, J. Zhou, Y. Ye, J. Wang and X. Wang, Kinetic investigation into pH-dependent color of anthocyanin and its sensing performance, *Dyes Pigm.*, 2019, **170**, 107643.
9 G. J. Khan, M. Jamshaid, M. I. Sajid, Z. U. Imtiaz, M. N. Majeed, F. A. Siddique, I. Bashir and N. Riaz, *Can. J. Appl. Sci.*, 2014, **4**, 66–80.
10 M. I. Gil, F. A. Tomás-Barberán, B. Hess-Pierce, D. M. Holcroft and A. A. Kader, *J. Agric. Food Chem.*, 2000, **48**, 4581–4589.
11 J. C. Beaulieu, S. W. Lloyd, J. E. Preece, J. W. Moersfelder, R. E. Stein-Chisholm and J. M. Obando-Ulloa, *Food Chem.*, 2015, **181**, 354–364.
12 J. M. Chater, D. J. Merhaut, Z. Jia, P. A. Mauk and J. E. Preece, *Sci. Hortic.*, 2017, **237**, 11–19.
13 A. Schaller, J. M. Chater, G. E. Vallad, J. Moersfelder, C. Heinitz and Z. Deng, *Horticulturae*, 2023, **9**, 1097.
14 T. R. Tohge and A. Fernie, *Mini-Rev. Med. Chem.*, 2017, **17**, 1013–1027.
15 L. Chen, R. Liu, J. Zhu, L. Wang, H. Li, J. Liu and Z. Lu, *Food Sci. Nutr.*, 2024, **12**, 6648–6659.
16 Z. P. Adams, J. Ehlting and R. Edwards, *J. Theor. Biol.*, 2019, **462**, 158–170.
17 A. Schieber and M. Wüst, *Molecules*, 2020, **25**, 4529.
18 A. Veithen, M. Philippeau and P. Chatelain, in *Springer Handbook of Odor*, ed. A. Buettner, Springer, Cham,

Switzerland, 1st edn, 2017, pp. 57–58, DOI: 10.1007/978-3-319-26932-0_22.
19 L. J. Chen and G. Hrazdina, *Phytochemistry*, 1981, **20**, 297–303.
20 J. Zhang, F. Giampieri, S. Afrin, M. Battino, X. Zheng and P. Reboredo-Rodriguez, *Int. J. Food Sci. Nutr.*, 2019, **70**, 285–293.
21 Y. Zhang, E. Butelli and C. Martin, *Curr. Opin. Plant Biol.*, 2014, **19**, 81–90.
22 K. Springob, J. I. Nakajima, M. Yamazaki and K. Saito, *Nat. Prod. Rep.*, 2003, **20**, 288–303.
23 X. Zhao, Z. Yuan, Y. Fang, Y. Yin and L. Feng, *Eur. Food Res. Technol.*, 2013, **236**, 109–117.
24 C. Mathon, J. M. Chater, A. Green, D. J. Merhaut, P. A. Mauk, J. E. Preece and C. K. Larive, *J. Sci. Food Agric.*, 2019, **99**, 4036–4042.
25 G. Qin, C. Xu, R. Ming, H. Tang, R. Guyot, E. M. Kramer, Y. Hu, X. Yi, Y. Qi, X. Xu and Z. Gao, *Plant J.*, 2017, **91**, 1108–1128.
26 T. Tanaka, G. I. Nonaka and I. Nishioka, *Phytochemistry*, 1985, **24**, 2075–2078.
27 S. A. Al-Harbi, A. O. Abdulrahman, M. A. Zamzami and M. I. Khan, *Front. Nutr.*, 2021, **8**, 647582.
28 L. Zhao, W. C. Chang, Y. Xiao, H. W. Liu and P. Liu, *Annu. Rev. Biochem.*, 2013, **82**, 497–530.
29 E. Vranová, D. Coman and W. Gruissem, *Annu. Rev. Plant Biol.*, 2013, **64**, 665–700.
30 R. S. N. Brilhante, É. P. Caetano, R. A. C. D. Lima, F. J. D. F. Marques, D. S. C. M. Castelo-Branco, C. V. S. D. Melo, G. M. D. M. Guedes, J. S. D. Oliveira, Z. P. D. Camargo, J. L. B. Moreira and A. J. Monteiro, *Braz. J. Microbiol.*, 2016, **47**, 917–924.
31 J. Chadha, L. Khullar, U. Mudgil and K. Harjai, *Fitoterapia*, 2024, **176**, 106051.
32 P. An, X. Yang, J. Yu, J. Qi, X. Ren and Q. Kong, *Food Control*, 2019, **98**, 42–53.
33 Z. Li, Y. Wei, Z. Cao, S. Jiang, Y. Chen and X. Shao, *J. Agric. Food Chem.*, 2021, **69**, 10678–10687.
34 F. Hilgers, S. S. Habash, A. Loeschcke, Y. S. Ackermann, S. Neumann, A. Heck, O. Klaus, J. Hage-Hülsmann, F. M. Grundler, K. E. Jaeger and A. S. S. Schleker, *Microorganisms*, 2021, **9**, 168.
35 Q. Wang, Z. Xin, J. Li, L. Hu, Y. Lou and J. Lu, *Physiol. Mol. Plant Pathol.*, 2015, **91**, 106–112.
36 R. A. Raguso, *Curr. Opin. Plant Biol.*, 2016, **32**, 31–36.
37 T. Okamoto, Y. Okuyama, R. Goto, M. Tokoro and M. Kato, *J. Evol. Biol.*, 2015, **28**, 590–600.
38 G. Benelli, A. Canale, D. Romano, G. Flamini, S. Tavarini, A. Martini, R. Ascrizzi, G. Conte, M. Mele and L. G. Angelini, *Arthropod-Plant Interact.*, 2017, **11**, 381–388.
39 K. J. Byers, H. D. Bradshaw Jr and J. A. Riffell, *J. Exp. Biol.*, 2014, **217**, 614–623.
40 L. Pecetti, A. Tava, A. Felicioli, M. Pinzauti and E. Piano, *Bull. Insectology.*, 2002, **55**, 21–28.
41 K. Mendonca, PhD Thesis, California Polytechnic State University, 2020, DOI: 10.15368/theses.2020.99.
42 I. Feussner and C. Wasternack, *Annu. Rev. Plant Biol.*, 2002, **53**, 275–297.
43 A. Z. Andreou, E. Hornung, S. Kunze, S. Rosahl and I. Feussner, *Lipids*, 2009, **44**, 207–215.
44 C. Wasternack, O. Miersch, R. Kramell, B. Hause, J. Ward, M. Beale, W. Boland, B. Parthier and I. Feussner, *Lipid/Fett*, 1998, **100**, 139–146.
45 L. D. Delgado, P. E. Zúñiga, N. E. Figueroa, E. Pastene, H. F. Escobar-Sepúlveda, P. M. Figueroa, A. Garrido-Bigotes and C. R. Figueroa, *Molecules*, 2018, **23**, 1433.
46 Y. Zhang and A. R. Fernie, *Adv. Biol.*, 2023, **7**, 2200238.
47 D. Jia, Z. Xu, L. Chen, Q. Huang, C. Huang, J. Tao, X. Qu and X. Xu, *J. Sci. Food Agric.*, 2023, **103**, 6055–6069.